JACS
JOURNAL OF THE AMERICAN CHEMICAL SOCIETY
pubs.acs.org/JACS
Article

# Metal–Metal Bonding in Actinide Dimers: $U_2$ and $U_2^-$

Sandra M. Ciborowski, Abhishek Mitra, Rachel M. Harris, Gaoxiang Liu, Prachi Sharma, Navneet Khetrapal, Moritz Blankenhorn, Laura Gagliardi,* and Kit H. Bowen*

Cite This: J. Am. Chem. Soc. 2021, 143, 17023–17028
Read Online
ACCESS | Metrics & More | Article Recommendations | Supporting Information

**ABSTRACT:** Understanding direct metal–metal bonding between actinide atoms has been an elusive goal in chemistry for years. We report for the first time the anion photoelectron spectrum of $U_2^-$. The threshold of the lowest electron binding energy (EBE) spectral band occurs at 1.0 eV, which corresponds to the electron affinity (EA) of $U_2$, whereas the vertical detachment energy of $U_2^-$ is found at EBE ∼ 1.2 eV. Electronic structure calculations on $U_2$ and $U_2^-$ were carried out with state-of-the-art theoretical methods. The computed values of EA($U_2$) and EA(U) and the difference between the computed dissociation energies of $U_2$ and $U_2^-$ are found to be internally consistent and consistent with experiment. Analysis of the bonds in $U_2$ and $U_2^-$ shows that while $U_2$ has a formal quintuple bond, $U_2^-$ has a quadruple bond, even if the effective bond orders differ only by 0.5 unit instead of one unit. The resulting experimental-computational synergy elucidates the nature of metal–metal bonding in $U_2$ and $U_2^-$.

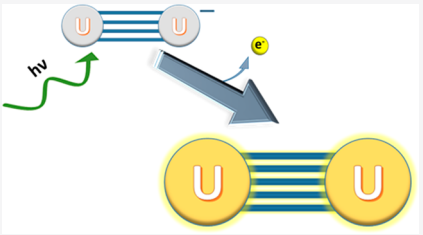




## INTRODUCTION

Actinide–actinide bonds are of fundamental interest in chemistry, with their bare metal dimers providing the simplest examples. Given the importance of uranium, there is significant interest in the uranium dimer, $U_2$. As a metal-to-metal molecular prototype, the uranium dimer exhibits purely covalent bonding, this being unusual among uranium-containing molecules. Moreover, as is often the case for actinides, the uranium dimer's electronic structure is exquisitely complex, prompting numerous theoretical studies.[1−8]

Over the past 15 years, debate has focused on the bonding scheme within the uranium dimer, $U_2$. Initially, as determined by Gagliardi and Roos, the ground state of $U_2$ was believed to have a quintuple bond, based on scalar complete active space self-consistent field (CASSCF) calculations, followed by perturbation theory (CASPT2), in which spin–orbit coupling was included a posteriori.[1] Their calculations revealed the following bonds between the two uranium atoms: three two-electron two-center bonds, i.e., one $\sigma_g$ and two $\pi_u$ from the 7s and 6d electrons, and four one-electron two-center bonds, i.e., one $\sigma_g$, one $\pi_u$, and two $\delta_g$ from 6d and 5f contributions, as well as two 5f electrons residing in nonbonding orbitals on each U atom.[1] This formally corresponds to a quintuple bond. Fourteen years later, Knecht, Jensen, and Saue[2] re-evaluated the bonding in $U_2$, finding its ground state to exhibit a quadrupole bond rather than the quintuple bond proposed by Gagliardi and Roos.[1] The Knecht et al. work was based on multiconfigurational CASSCF calculations using the same active space as in the calculation by Gagliardi and Roos,[1] but included variational spin–orbit coupling.[2,9] Moreover, they also concluded that the previously calculated quintuple ground state is instead a low-lying electronically excited state.[2] The electronic ground state was shown to consist of three electron-pair bonds, i.e., one $\sigma$ and two $\pi$, two one-electron bonds of $\sigma$ and $\delta$ types, and four coupled 5f electrons localized on each U atom.[2] Without experimental validation, the debate remained ongoing.

In view of the above, we aim to resolve the long-debated bonding scheme in $U_2$ using the synergy between negative ion photoelectron spectroscopy and state-of-the-art quantum chemical calculations. We report joint experimental and theoretical investigations of the $U_2^-$ anion. Together, these reveal the electronic structure and chemical bonding scheme of neutral $U_2$, this being facilitated by the photodetachment of the excess electron in the $U_2^-$ anion to yield the ground and various electronic states of the neutral $U_2$ molecule. Thus, while the experiments are conducted on $U_2^-$, i.e., on the anion, the results largely pertain to the electronic states of $U_2$, i.e., the anions' neutral counterpart. The resulting anion photoelectron spectrum of $U_2^-$, reported here for the first time, provides the experimental benchmark upon which high-level electronic structure calculations are validated. Together, this combined experimental and theoretical study elucidates the nature of chemical bonding in $U_2$ and $U_2^-$.

## METHODS

**Experimental Methods.** Anion photoelectron spectroscopy is conducted by crossing a beam of mass-selected negative ions with a

Received: June 21, 2021
Published: October 5, 2021




https://doi.org/10.1021/jacs.1c06417
J. Am. Chem. Soc. 2021, 143, 17023–17028

fixed-frequency photon beam and energy-analyzing the resultant photodetached electrons. The photodetachment process is governed by the energy-conserving relationship: $h\nu$ = EBE + EKE, where $h\nu$ is the photon energy, EBE is the electron binding (photodetachment transition) energy, and EKE is the electron kinetic energy. Our apparatus consists of a laser vaporization cluster anion source, a time−of−flight mass spectrometer, a Nd:YAG photodetachment laser, and a magnetic bottle electron energy analyzer.[10] The magnetic bottle photoelectron spectrometer resolution is ∼35 meV at EKE = 1 eV. In this study, the third (355 nm, 3.49 eV) harmonic output of a Nd:YAG laser was used to photodetach electrons from mass−selected uranium cluster anions, $U_n^-$ (n = 2−8). The well−known atomic transitions of $Cu^-$ were used to calibrate the magnetic bottle spectra.[10]

The uranium dimer anions were generated in a laser vaporization ion source. Figure 1 presents a schematic of this source. Briefly, a

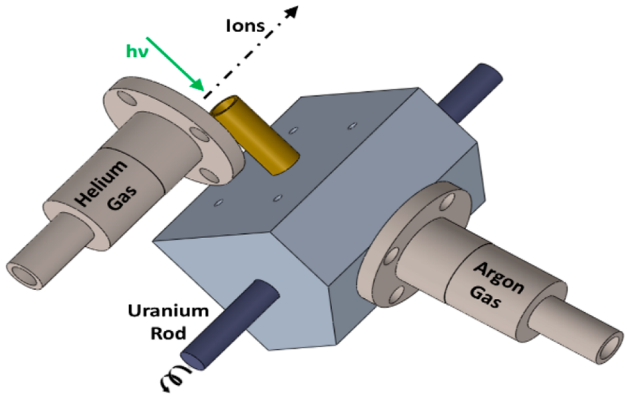


**Figure 1.** Schematic of the two-stage laser vaporization source used to generate the $U_2^-$.

housed, rotating, and translating uranium rod was ablated using the second harmonic (532 nm, 2.66 eV) of a Nd:YAG laser, while 60 psig of argon gas was pulsed over the rod. A second pulsed valve, backed with 100 psig of helium gas, introduced the anions to the TOF-MS, from which the anions were mass-gated before their electrons were photodetached and energy-analyzed.

Additional uranium cluster anions, $U_n^-$ (n = 3−8), were created in a more traditional laser vaporization source. The second harmonic photon pulses ablated the rotating, translating uranium rod and directly introduced the ions into the TOF-MS, prior to the ions being mass-gated and their electrons energy-analyzed. The anion photoelectron spectra of $U_n^-$ (n = 3−8) are presented in Figure S1.

**Theoretical Methods.** Single point energy calculations were performed using the complete active space self-consistent field (CASSCF) method[11] for both $U_2$ and $U_2^-$ at various bond distances near their equilibrium geometry. The active space employed consists of 6 and 7 valence electrons for $U_2$ and $U_2^-$, respectively, in 21 orbitals. Dynamical correlation effects were incorporated using the complete active space second order perturbation theory (CASPT2) on top of the CASSCF wave functions. The energies for excited electronic states were calculated at the multistate complete active space second order perturbation theory (MS-CASPT2) level of theory.[12,13] The OpenMolcas software package[14] was used to perform all the calculations. Scalar relativistic effects were incorporated by using the Douglas−Kroll−Hess (DKH) Hamiltonian.[15−17] The spin−orbit coupling effects were incorporated by using the SO-RASSI module[18] available in OpenMolcas. Atomic natural orbital type basis set[19] were used. A primitive set 26s23p17d13f5g3h was contracted to 9s8p6d4f2g. In order to maintain a linear geometry, a $D_{2h}$ symmetry and the keyword "Linear" was used to impose supersymmetry. In total, 240 octet states lying up to 0.56 eV above the ground state, 80 sextet states lying up to 0.62 eV above the ground state, 30 quartet states lying up to 0.81 eV above the ground state, and 10 doublet states lying up to 0.85 eV above the ground state were allowed to interact using the spin−orbit coupling Hamiltonian. In order to find the electronic ground state, the electronic energies for some points near the equilibrium geometry of $U_2^-$ for the resulting 2540 spin−orbit coupled states were calculated and compared. In order to calculate the dissociation energies, the absolute energies for the U and $U^-$ atoms are calculated at the CASSCF level of theory by averaging over 17 and 38 states, respectively. As was done for the dimers, dynamical correlation effects for the atoms are similarly incorporated using MS-CASPT2. For the atoms, a $D_2$ symmetry was considered and the keyword "Atom" was used to impose supersymmetry. Active spaces containing 6 and 7 valence electrons in 16 orbitals were employed for U and $U^-$, respectively. The 16 orbitals considered here correspond to one 7s, three 7p, five 6d, and seven 5f orbitals. In total, for the $U^-$ atomic specie, 152 octet states lying up to 2.02 eV above the ground state, 152 sextet states lying up to 0.85 eV above the ground state, and 152 quartet states lying up to 1.16 eV above the ground state were allowed to interact using the spin−orbit coupling Hamiltonian. For the U atom, 68 septet states lying up to 1.44 eV above the ground state, 68 pentet states lying up to 0.82 eV above the ground state, and 68 triplet states lying up to 1.05 eV above the ground state were allowed to interact using the spin−orbit coupling Hamiltonian. The energies of the atomic species were used to calculate the absolute energy of the $U_2$ and at infinite bond distances. An imaginary shift of 0.2 and the default ionization potential electron affinity (IPEA)[20] of 0.25 were employed. The IPEA is an empirical correction applied to the zero-order Hamiltonian.

## RESULTS AND DISCUSSION

**Experimental Results.** Atomic uranium cations, $U^+$, have long been observed in mass spectra along with various uranium oxide and hydride cationic stoichiometries.[21−23] To prepare the gas-phase uranium dimer anion, $U_2^-$, we initially employed a conventional (one stage) laser-vaporization source in which a pulsed laser beam ablated a depleted uranium rod to generate a plasma, which was propelled forward by a jet of supersonically expanding helium gas. While this method made copious intensities of $U_mO_n^-$ cluster anions for $m \geq 2$ and weaker signals of $U_m^-$ cluster anions for $m \geq 3$, $U_2^-$ was essentially absent (see Figure 2A). The likely culprit was the oxidized surface of the uranium rod, which provided oxygen to the plasma during laser-vaporization, in turn reacting with the $U_m^-$ cluster anions to form $U_mO_n^-$ cluster anions. Because bare metal clusters readily react to form metal oxide cluster anions, the latter's signals prevailed in the mass spectrum, reducing the formation of $U_m^-$ and especially of $U_2^-$. To suppress the effects of oxygen, we then used a two-stage (compound) laser vaporization source,[24] in which two pulsed beams are crossed (see Figure 1). The beam formed by laser vaporization of the uranium rod is perpendicular to the other beam's path which itself continues on into the main apparatus and into the anion extraction region of the time-of-flight mass analyzer/selector. The plasma formed during laser vaporization of the uranium rod is propelled by pulses of argon gas to reduce the velocities of the constituent species in that beam. The other beam is a pulsed helium jet.

The large mass differences between uranium clusters and oxidized uranium clusters caused them to travel at different speeds coming out of the laser vaporization source. By controlling the timing of the second (helium) pulsed valve, different species ions were preferentially entrained by the helium expansion, where collisional cooling and dimer anion formation were promoted. Figure 2B shows a typical mass spectrum obtained by using this two-stage source. The uranium dimer anion, $U_2^-$ is observed at a significant intensity, while the formation of uranium oxide anions is significantly reduced.


https://doi.org/10.1021/jacs.1c06417
J. Am. Chem. Soc. 2021, 143, 17023−17028

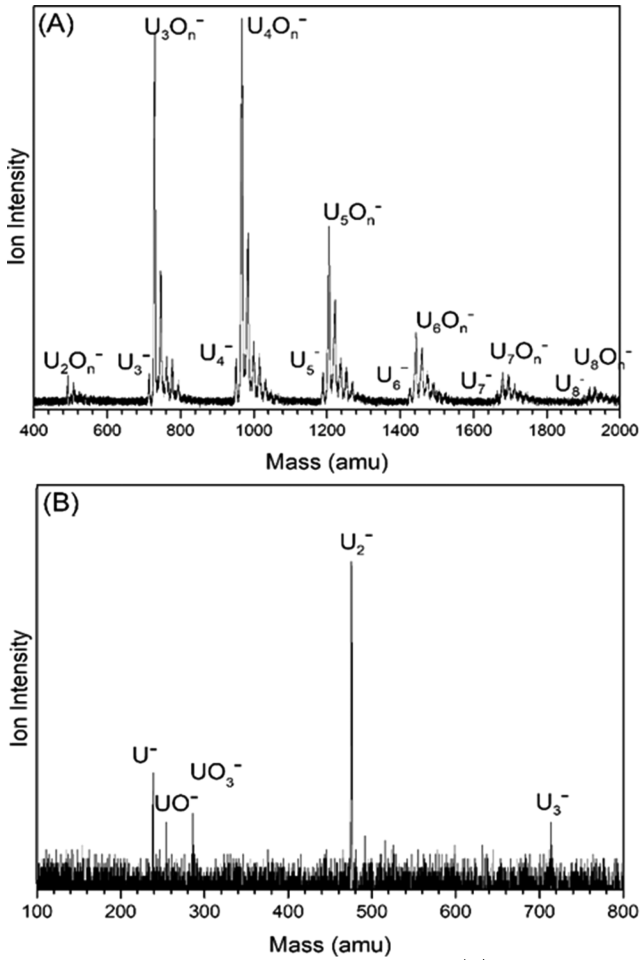


**Figure 2.** Mass spectra resulting from the use of (A) a conventional (one-stage) laser vaporization source versus (B) using a two-stage laser vaporization source.

Figure 3 presents the negative ion photoelectron spectrum of $U_2^-$ recorded with 3.49 eV (355 nm) photons using a magnetic bottle electron energy analyzer. The lowest electron binding energy (EBE) band in the spectrum exhibits a sharp threshold at 1.0 eV and an intensity maximum between EBE = 1.1 and 1.3 eV. When there is sufficient Franck–Condon overlap between the ground state of the anion and the ground state of the neutral species, and when there is negligible hot band (vibrationally excited anion) signal, the threshold of the first EBE band signifies the electron affinity (EA) determining transition. The vertical detachment energy (VDE) is the photodetachment transition energy at which the Franck–Condon overlap between the electronic ground-state wave functions of the anion and its neutral counterpart is maximal, here, corresponding to EBE ~ 1.2 eV. Thus, the EA value for neutral $U_2$ is revealed to be 1.0 eV, while the VDE value of the $U_2^-$ anion is found to be ~1.2 eV. A weak signal observed at EBE ~ 0.4 eV is likely due to the subsequent photodetachment of $U^-$, itself generated by the photodissociation of $U_2^-$, as this value was observed in our previous study of the atomic uranium anion.[25] Features present at higher EBE values correspond to photodetachment transitions to the excited vibrational and electronic states of neutral $U_2$. The spectral pattern observed in Figure 3 suggests the presence of numerous under-lying unresolved transitions.

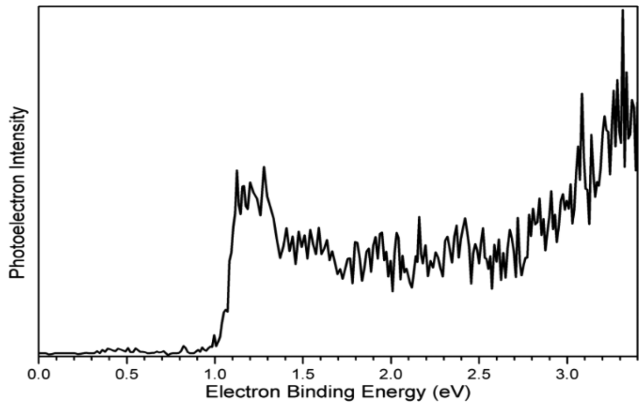


**Figure 3.** Anion Photoelectron Spectrum of the Uranium Dimer Anion, $U_2^-$. This spectrum was measured using the third harmonic (355 nm, 3.49 eV) of a Nd:YAG laser.

**Theoretical Results.** The experimentally determined adiabatic electron affinity (EA) of the uranium dimer is compared to the theoretically computed value obtained from state-of-the art electronic structure theory calculations on $U_2$ and $U_2^-$. Multireference wave function calculations of the state-averaged complete active space self-consistent field (CASSCF) type,[11] followed by a multistate second order perturbation theory (MS-CASPT2) treatment[12,13] to account for both static and dynamic correlation effects, were performed to determine electronic energies (Figure 4) at bond distances

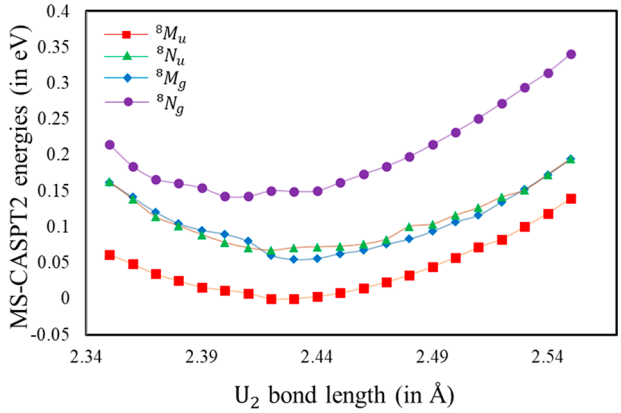


**Figure 4.** MS-CASPT2 potential energy curves for the lowest-lying electronic states of $U_2^-$ near its equilibrium geometry.

near the equilibrium bond distances of the $U_2$ and $U_2^-$ systems. The ground state for $U_2$ is determined as $^7O_g$ ($8_g$) (without and with spin–orbit coupling notations) which is in agreement with the reported ground state.[1] It should be noted that although Knecht et al.[2] used fully relativistic CASSCF calculations to determine $9_g$ as the electronic ground state and $8_g$ as a low-lying excited state, their calculations did not include dynamical correlation effects, which are required to fully understand the electronic structure of $U_2$. (More details are available in SI.)

In similarity to $U_2$, for $U_2^-$, the highest spin state, i.e., the octet, is found to be the most stable electronic state with an angular momentum ($\Lambda$) of 9 au and ungerade symmetry. The wave function for the ground state of $U_2^-$ can be expressed as a linear combination of two dominant configurations


https://doi.org/10.1021/jacs.1c06417
J. Am. Chem. Soc. 2021, 143, 17023–17028

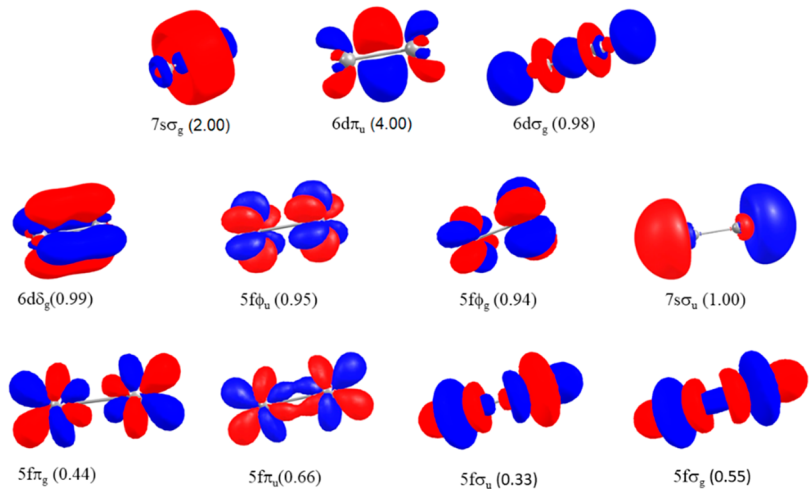


**Figure 5.** Active molecular orbitals along with the number of electrons occupying the orbitals (in brackets) for the uranium dimer anion.

$$\psi = \mathbf{0.736}(7s\sigma_g)^2(6d\pi_u)^4(6d\sigma_g)^1(6d\delta_g)^1(5f\sigma_g)^1(5f\pi_u)^1(5f\phi_u)^1(5f\phi_g)^1(7s\sigma_u)^1 \;\&$$
$$\mathbf{0.560}(7s\sigma_g)^2(6d\pi_u)^4(6d\sigma_g)^1(6d\delta_g)^1(5f\sigma_u)^1(5f\pi_g)^1(5f\phi_u)^1(5f\phi_g)^1(7s\sigma_u)^1 \quad (1)$$

as well as other nondominant terms.

The bonding in $U_2^-$ can be understood in terms of an effective bond order $E_{ebo}$ defined as in eq 2.

$$E_{ebo} = \frac{1}{2}\sum_i (n_{be_i} - n_{abe_i}) \quad (2)$$

Here, $n_{be_i}$ and $n_{abe_i}$ represent the electron occupation numbers in the $i^{th}$ pair of bonding and antibonding natural orbitals, respectively. Furthermore, the summation runs over all pairs of bonding and antibonding orbitals. The calculations indicate that $U_2^-$ has a formal quadrupole bond corresponding to a calculated effective bond order of 3.7. The natural orbitals providing the main contributions to forming $U_2^-$ are presented in Figure 5 along with their respective occupation numbers.

The wave function for the ground state of $U_2$ can be expressed as a linear combination of two dominant configurations as was shown by Gagliardi et al.:[1]

$$\psi = \mathbf{0.774}(7s\sigma_g)^2(6d\pi_u)^4(6d\sigma_g)^1(6d\delta_g)^1(5f\pi_u)^1(5f\delta_g)^1(5f\phi_u)^1(5f\phi_g)^1 \;\&$$
$$\mathbf{0.597}(7s\sigma_g)^2(6d\pi_u)^4(6d\sigma_g)^1(6d\delta_g)^1(5f\pi_g)^1(5f\delta_u)^1(5f\phi_u)^1(5f\phi_g)^1 \quad (3)$$

as well as other nondominant terms. As seen in eq 1, the antibonding $7s\sigma_u$ orbital is occupied in all the dominant configurations of $U_2^-$, thereby resulting in a decrease in bond order. Thus, according to our analysis, $U_2$ has a formal weak quintuple bond with a bond order of 4.2, whereas $U_2^-$ has a formal quadrupole bond with a bond order of 3.7. The formal bond orders of the two molecules differ by one unit, but the effective bond orders differ by 0.5 unit. It should be noted that although the $7s\sigma_u$ orbital has been assigned as "anti-bonding" from symmetry considerations, it has some non-bonding character. A detailed discussion on this is provided in the SI.

Both scalar relativistic effects and spin−orbital coupling have been accounted for. Scalar relativistic effects are introduced through one-body terms in the Douglas−Kroll−Hess (DKH) Hamiltonian.[15−17] Moreover, spin−orbit (SO) coupling is added as a posteriori correction to DKH and calculated by allowing fully optimized CASSCF states to interact under a SO Hamiltonian along with a shift in the diagonal terms to account for dynamic correction added through perturbation theory. This indicates that the effects caused due to the coupling of electronic and spin states are similar for the two species and therefore cancel out. The equilibrium distances for $U_2$ and $U_2^-$ are found to be 2.42 and 2.43 Å, respectively. This is consistent with a photoelectron origin band that is devoid of an extended vibrational progression. The harmonic vibrational frequencies for the ground state of $U_2$ and $U_2^-$ are calculated to be 265 and 220 $cm^{-1}$, respectively, too small to have been resolved in the present experiment. The calculated EA value of the uranium dimer, $U_2$, is found to be 0.71 eV (see Table S2). This computed EA value is lower than the experimentally obtained electron affinity by 0.29 eV. We observed that even though the spin−orbit-coupling effects play a major role in altering the absolute bond energies of the uranium dimer and uranium dimer anion, they have a minimal contribution in changing the electron affinity. Our theoretical calculations predict $U_2^-$ to have both a higher dissociation energy and a lower absolute energy than the uranium dimer, $U_2$, consistent with its occurrence and observation in the gas phase.

## CONCLUSIONS

The original computational determination by Gagliardi and Roos,[1] that the ground state of $U_2$ is characterized by a quintuple bond, was challenged by the computational work of Knecht, Jensen, and Saue,[2] who instead found the ground state of $U_2$ to be described as possessing a quadrupole bond. The present work has two synergetic parts. Its new, higher level computations confirmed the original $U_2$ quintuple bond conclusion of Gagliardi and Roos and also found $U_2^-$ to possess a quadrupole bond. Its experimental arm measured the anion photoelectron spectrum of $U_2^-$, thus providing the electron affinity of neutral $U_2$. A comparison of its experimentally determined EA($U_2$) value, i.e., 1.0 eV, with its computationally determined EA($U_2$) value, i.e., 0.71 eV, largely supported our calculations. Because electronic structure calculations on the uranium dimer, $U_2$, and its anion, $U_2^-$, are extraordinarily demanding, perfect agreement would have been a high bar. Another way to validate our computational results is to calculate the dissociation energies of $U_2^-$ and $U_2$ and to take their difference. An energetic cycle shows that $EA(U_2) - EA(U) = D_0(U_2^-) - D_0(U_2)$. The knowledge that EA($U_2$) = 1.0 eV, from our present experimental work, and


https://doi.org/10.1021/jacs.1c06417
J. Am. Chem. Soc. 2021, 143, 17023−17028

that EA(U) = 0.31 eV, from our recent experimental work,[25,26] implies that $D_0(U_2^-) - D_0(U_2)$ is 0.69 eV. The difference between separately calculated $D_0(U_2^-)$ and $D_0(U_2)$ values in this work is 0.61 eV, in close accord with the expected value. Table S6 summaries several calculated properties of $U_2$ and $U_2^-$. Even if both calculated $EA(U_2)$ and EA(U) values differ from the experimental ones by about 0.3 eV, the calculated difference, $EA(U_2) - EA(U)$, agrees well with the experimental one because of error cancellation.

## ■ ASSOCIATED CONTENT

### Supporting Information

The Supporting Information is available free of charge at https://pubs.acs.org/doi/10.1021/jacs.1c06417.

Calculation details, theoretical, and experimental results (PDF)

## ■ AUTHOR INFORMATION


### Corresponding Authors

**Laura Gagliardi** − *Department of Chemistry, Pritzker School of Molecular Engineering, James Franck Institute, Chicago Center for Theoretical Chemistry, The University of Chicago, Chicago, Illinois 60637, United States;* Present Address: Argonne National Laboratory, Illinois 60439, United States; orcid.org/0000-0001-5227-1396; Email: kbowen@ jhu.edu

**Kit H. Bowen** − *Department of Chemistry, Johns Hopkins University, Baltimore, Maryland 21218, United States;* orcid.org/0000-0002-2858-6352; Email: lgagliardi@ uchicago

### Authors

**Sandra M. Ciborowski** − *Department of Chemistry, Johns Hopkins University, Baltimore, Maryland 21218, United States;* orcid.org/0000-0001-9453-4764

**Abhishek Mitra** − *Department of Chemistry, Pritzker School of Molecular Engineering, James Franck Institute, Chicago Center for Theoretical Chemistry, The University of Chicago, Chicago, Illinois 60637, United States;* orcid.org/0000-0002-2974-9600

**Rachel M. Harris** − *Department of Chemistry, Johns Hopkins University, Baltimore, Maryland 21218, United States;* orcid.org/0000-0002-3585-5258

**Gaoxiang Liu** − *Department of Chemistry, Johns Hopkins University, Baltimore, Maryland 21218, United States;* orcid.org/0000-0002-1001-0064

**Prachi Sharma** − *Department of Chemistry, University of Minnesota, Minneapolis, Minnesota 55455, United States;* orcid.org/0000-0002-1819-542X

**Navneet Khetrapal** − *Department of Chemistry, University of Minnesota, Minneapolis, Minnesota 55455, United States*

**Moritz Blankenhorn** − *Department of Chemistry, Johns Hopkins University, Baltimore, Maryland 21218, United States*

Complete contact information is available at: https://pubs.acs.org/10.1021/jacs.1c06417


### Author Contributions

The manuscript was written through contributions of all authors.

### Notes

The authors declare no competing financial interest.

## ■ ACKNOWLEDGMENTS

The experimental part of this material was supported by the U.S. Department of Energy (DOE), Office of Science, Basic Energy Sciences, Heavy Element Chemistry program under award number DE-SC0019317 (K.H.B.). The theoretical calculations are based on work supported by the U.S. Department of Energy (DOE), Office of Basic Energy Sciences, Division of Chemical Sciences, Geosciences, and Biosciences under grant no. USDOE/DE-SC002183 (L.G.). This work was completed with computing resources provided by the Minnesota Supercomputing Institute (MSI) and University of Chicago Research Computing Center (L.G.).

## ■ REFERENCES


(1) Gagliardi, L.; Roos, B. O. Quantum Chemical Calculations Show That the Uranium Molecule $U_2$ Has a Quintuple Bond. *Nature* **2005**, *433* (7028), 848−851.

(2) Knecht, S.; Jensen, H. J. A.; Saue, T. Relativistic Quantum Chemical Calculations Show That the Uranium Molecule $U_2$ Has a Quadruple Bond. *Nat. Chem.* **2019**, *11* (1), 40−44.

(3) Roos, B. O.; Malmqvist, P. Å.; Gagliardi, L. Exploring the Actinide-Actinide Bond: Theoretical Studies of the Chemical Bond in $Ac_2$, $Th_2$, $Pa_2$, and $U_2$. *J. Am. Chem. Soc.* **2006**, *128* (51), 17000.

(4) Gagliardi, L.; Roos, B. O. Multiconfigurational Quantum Chemical Methods for Molecular Systems Containing Actinides. *Chem. Soc. Rev.* **2007**, *36* (6), 893−903.

(5) Bursten, B. E.; Ozin, G. A. X$\alpha$-SW Calculations for Naked Actinide Dimers: On the Existence of Φ Bonds Between Metal Atoms. *Inorg. Chem.* **1984**, *23* (18), 2910−2911.

(6) Pepper, M.; Bursten, B. E. Ab Initio Studies of the Electronic Structure of the Diuranium Molecule. *J. Am. Chem. Soc.* **1990**, *112* (21), 7803−7804.

(7) Erkoç, Ş.; Baştuğ, T.; Hirata, M.; Tachimori, S. Molecular-Dynamics Simulations of Uranium Microclusters. *J. Phys. Soc. Jpn.* **1999**, *68* (2), 440−445.

(8) Gingerich, K. A. Experimental and Predicted Stability of Diatomic Metals and Metallic Clusters. In *Faraday Symp. Chem. Soc.*; The Royal Society of Chemistry, 1980; Vol. *14*, pp 109−125.

(9) Lemonick, S. Uranium Dimer Loses a Bond. *C&EN Glob. Enterp.* **2018**, *96* (45), 9−9.

(10) Ho, J.; Ervin, K. M.; Lineberger, W. C. Photoelectron Spectroscopy of Metal Cluster Anions: $Cu_n^-$, $Ag_n^-$, and Aun-. *J. Chem. Phys.* **1990**, *93* (10), 6987−7002.

(11) Roos, B. O. The Complete Active Space Self-Consistent Field Method and Its Applications in Electronic Structure Calculations. In *AB Initio Methods in Quantum Chemistry - II*; Wiley: 2007; Vol. *69*, pp 399−445.

(12) Andersson, K.; Malmqvist, P. Å.; Roos, B. O.; Sadlej, A. J.; Wolinski, K. Second-Order Perturbation Theory with a CASSCF Reference Function. *J. Phys. Chem.* **1990**, *94* (14), 5483−5488.

(13) Finley, J.; Malmqvist, P. Å.; Roos, B. O.; Serrano-Andrés, L. The Multi-State CASPT2Method. *Chem. Phys. Lett.* **1998**, *288* (2−4), 299−306.

(14) Fdez, I. G; Vacher, M.; Alavi, A.; Angeli, C.; Aquilante, F.; Autschbach, J.; Bao, J. J.; Bokarev, S. I.; Bogdanov, N. A.; Carlson, R. K.; et al. OpenMolcas: From Source Code to Insight. Journal of Chemical Theory and Computation. *J. Chem. Theory Comput.* **2019**, *12*, 5925−5964.

(15) Douglas, M.; Kroll, N. M. Quantum Electrodynamical Corrections to the Fine Structure of Helium. *Ann. Phys. (Amsterdam, Neth.)* **1974**, *82* (1), 89−155.

(16) Hess, B. A. Relativistic Electronic-Structure Calculations Employing a Two-Component No-Pair Formalism with External-Field Projection Operators. *Phys. Rev. A: At., Mol., Opt. Phys.* **1986**, *33* (6), 3742−3748.

(17) Heß, B. A.; Marian, C. M.; Wahlgren, U.; Gropen, O. A Mean-Field Spin-Orbit Method Applicable to Correlated Wavefunctions. *Chem. Phys. Lett.* **1996**, *251* (5−6), 365−371.
(18) Malmqvist, P. Å.; Roos, B. O.; Schimmelpfennig, B. The Restricted Active Space (RAS) State Interaction Approach with Spin-Orbit Coupling. *Chem. Phys. Lett.* **2002**, *357* (3−4), 230−240.
(19) Almlöf, J.; Taylor, P. R. General Contraction of Gaussian Basis Sets. I. Atomic Natural Orbitals for First- and Second-Row Atoms. *J. Chem. Phys.* **1987**, *86* (7), 4070−4077.
(20) Ghigo, G.; Roos, B. O.; Malmqvist, P. Å. A Modified Definition of the Zeroth-Order Hamiltonian in Multiconfigurational Perturbation Theory (CASPT2). *Chem. Phys. Lett.* **2004**, *396* (1−3), 142−149.
(21) Gorokhov, L. N.; Emelyanov, A. M.; Khodeev, Y. S. Mass-Spectroscopic Investigation of Stability of Gaseous Molecules of $U_2O_2$ and $U_2$. *High Temp.* **1974**, *12* (6), 1156−1158.
(22) Heaven, M. C.; Barker, B. J.; Antonov, I. O. Spectroscopy and Structure of the Simplest Actinide Bonds. *J. Phys. Chem. A* **2014**, *118* (46), 10867−10881.
(23) Devienne, F. M.; Combarieu, R.; Teisseire, M. Action of Different Gases, Specially Nitrogen, on the Formation of Uranium Clusters; Comparison with Niobium and Tantalum Clusters. *Surf. Sci.* **1981**, *106* (1−3), 204−211.
(24) Lu, Y. J.; Lehman, J. H.; Carl Lineberger, W. A Versatile, Pulsed Anion Source Utilizing Plasma-Entrainment: Characterization and Applications. *J. Chem. Phys.* **2015**, *142* (4), 44201.
(25) Ciborowski, S. M.; Liu, G.; Blankenhorn, M.; Harris, R. M.; Marshall, M. A.; Zhu, Z.; Bowen, K. H.; Peterson, K. A. The Electron Affinity of the Uranium Atom. *J. Chem. Phys.* **2021**, *154* (22), 224307.
(26) Liu, G.; Ciborowski, S. M.; Bowen, K. H. Photoelectron Spectroscopic and Computational Study of Pyridine-Ligated Gold Cluster Anions. *J. Phys. Chem. A* **2017**, *121* (31), 5817−5822.


https://doi.org/10.1021/jacs.1c06417
*J. Am. Chem. Soc.* 2021, 143, 17023−17028